ELSEVIER

Contents lists available at ScienceDirect

Building and Environment

journal homepage: www.elsevier.com/locate/buildenv





Effect of room size, shape, AC placement, and air leakage on indoor airborne viral transmission

K. Choudhary a, K.A. Krishnaprasad b, N. Zgheib c,*, M.Y. Ha a, S. Balachandar b

- ^a School of Mechanical Engineering, Pusan National University, Busan, Republic of Korea
- ^b Department of Mechanical and Aerospace Engineering, University of Florida, Gainesville, FL 32611, USA
- ^c Department of Mechanical Engineering, The University of Texas Rio Grande Valley, Edinburg, TX 78539, USA

ARTICLE INFO

Keywords: COVID-19 Indoor viral transmission Pathogen concentration Room shape AC location

ABSTRACT

We conducted Euler–Lagrange Reynolds-Averaged Navier–Stokes simulations with statistical overloading to investigate the effect of room shape, air-condition (AC) location, and the presence of an open window on indoor airborne viral transmission, particularly as it relates to the spatio-temporal distribution of viral-laden droplet nuclei. Two room geometries were considered with two different AC types positioned at different locations within each room. We considered the case of perfect filtration where pathogens can exit the room through ventilation, air leakage through an open window, turbulent wall deposition, and by gravitational settling onto the bottom floor. We observe the room-averaged concentration to decay at the rate estimated from the well-mixed model and therefore to be independent of room size and shape or AC type and placement. It is also independent of whether or not there is an open window. However, we find that the departure from well-mixedness, which has been quantified using a time- and source-to-sink separation-dependent correction function γ , is affected by room shape and AC placement. More specifically, indoor spaces where the AC is installed on one end of the room allow droplet nuclei ejected on one end of the room to travel longer distances before being removed from the room as opposed to indoor spaces in which the AC is installed at the center of the room. The present results allow generalization of a simple model for the accurate prediction of viral quanta inhaled by an individual in any indoor environment.

1. Introduction

The Covid-19 pandemic has devastated communities across the world. Aside from the staggering death toll, and the health implications suffered by those infected by the virus, the economic repercussions were detrimental. These repercussions came about primarily by the often-necessary health measures, which lead to shutdowns and closures of all but a few essential industries and sectors. Other measures such as imposing occupancy limits and requiring individuals to maintain a certain separation from one another (i.e. social distancing) were also implemented [1–5]. The closures and the above mandates were driven by the desire to reduce the virus transmission, especially in indoor settings where the risk was highest [6–8].

While the viral transmissibility is a complex statistical phenomenon that requires multidisciplinary knowledge, an essential element involves fluid mechanics, namely the spatio-temporal distribution of virus-laden droplet nuclei within enclosed spaces [9–18]. A key component thus in reducing the risk of airborne virus transmission is to optimize the design of new construction including restaurants, office

spaces, and household rooms [19–24]. The new optimized designs would aim at reducing the concentration of aerosols under various operating conditions; this includes proper placement and operation of the ventilation system. Furthermore, in the case of existing construction, it is worthwhile to understand how modifications to the ventilation system could enhance indoor air quality.

From a fluid mechanics perspective, such an optimization process remains a daunting task due to the countless possibilities that need to be explored. For instance, optimization must consider all possible locations of the sick individual(s) (source) and susceptible receiver(s) (sink) in the room, all possible expiration activities by the sick individual(s), operating conditions of the air conditioner (its air speed, temperature, and humidity settings). An exhaustive investigation of all such possibilities with a brute force approach of many different simulations, clearly, is out of the question. For instance, the vast majority of work on room-scale fluid mechanics of airborne transmission, both experimental and numerical, consider the case where pathogens or particles of a certain size distribution are released at a particular

E-mail address: nadim.zgheib@utrgv.edu (N. Zgheib).

Corresponding author.

rate from a source that is fixed at a particular location in a room [25–28]. Additionally, sensors are placed at various specific locations to measure the temporal evolution of the pathogen/particle concentration. While such studies are useful, they only provide information for those specific source/sink combinations. To obtain information for other source/sink combinations, the pathogen source and sink locations need to be changed accordingly, and the experiment/simulation needs to be repeated.

To overcome the aforementioned limitations, Salinas et al. (2022) [29] recently proposed a novel technique for addressing this fluid mechanics problem using a statistical overloading technique, combined with a scaling analysis that collapses the effects of the operating conditions of the air conditioner. The statistical overloading technique consisted of releasing, and individually tracking, tens of millions of airborne droplet nuclei of various sizes, far in excess of what could be present in a typical indoor setting (i.e., from a typical expiratory activity such as breathing, conversing, singing, etc.) [30]. Simulations with such a large number of nuclei was possible due to the one-way coupled nature of the problem (i.e., the airborne nuclei do not alter the room-scale flow). By distributing a large number of nuclei over the entire indoor space it was possible to provide statistically relevant results for every possible source-sink combination, with a single large eddy simulation. Furthermore, they showed that the results for different ventilation intensities, measured in terms of air changes per hour (ACH), can be perfectly scaled. Their analysis provided an easy-to-use correction function that could be used in conjunction with the well-mixed model of Bazant & Bush [31], thereby taking into account physiological and epidemiological factors such as droplet ejection rate by the sick individual, viral infectivity, etc.

In summary, with the above mentioned simplifications, the statistical information on the quanta of viral load inhaled by a susceptible individual can be readily obtained in terms of the well-mixed theory and the source–sink separation distance-dependent correction function. The only parameters to be still explored are the shape and size of the room, location of the air conditioner within the room, and other details such as open windows. However, even a limited number of the high-fidelity, statistically-overloaded large-eddy simulations (LES) remain computationally expensive. A valid alternative is to use Reynolds-Averaged Navier–Stokes (RANS) simulations. In fact, Choudhary et al. [32] conducted a critical evaluation of RANS against the high-fidelity LES simulations and showed that the former can be used to provide accurate estimates for the spatio-temporal concentration of airborne droplet nuclei.

The purpose of this paper is to build upon the recent findings of [29,32] to investigate the effect of room geometry and placement of the ventilation system on nuclei concentration. More specifically, we will consider four different cases corresponding to two room shapes. We varied several parameters including the placement of the ventilation system, the number and size of inlets and outlets, as well as the presence of an open window. In particular, we will focus on the following two aspects: (i) The earlier LES and RANS simulations had demonstrated that the well-mixed model provides an excellent approximation for the room-averaged pathogen concentration. In this work, we will examine how this result on room-averaged pathogen concentration is affected by the room geometry and placement of room ventilation. (ii) We will also assess how the room geometry affects departure from wellmixedness as well as average pathogen concentration at the location of the susceptible individual for a prescribed separation distance from the sick individual. Together, these two pieces of information will allow us to properly quantify the effect of room shape and placement of room ventilation. We perform four different RANS simulations with statistical overloading to obtain these results.

2. Numerical setup and mathematical formulation

The baseline physical setup under consideration consists of a 4way air-conditioning (AC) system installed at the center of the ceiling of a canonical room with dimensions of 10 m \times 10 m \times 3.2 m. The 4-way air-conditioning system comprises a pressure outlet (60 cm \times 60 cm) surrounded by four velocity inlets of rectangular cross section (5.5 cm \times 44 cm). The configuration can be seem in Fig. 1C.

We solve the Reynolds-Averaged Navier-Stokes equations with the $k-\varepsilon$ realizable model. Details of the numerical methodology can be found in [32]. Here we provide a brief summary for completeness. We use a structured grid with a relatively fine resolution near the outer surfaces of the numerical domain and a relatively coarse resolution in the interior. A total of 15 inflation layers are assigned near the walls with the thickness of the first grid layer set at 0.5 mm and the growth rate set at 1.5. A fine resolution is necessary near the outer surfaces to resolve the large velocity gradients. The no-slip and no-penetration boundary condition is imposed on all surfaces except for the four inlets and outlet. The outlet is set as a pressure outlet and the inlets are oriented at 40 degrees with respect to the ceiling. For the inlets, a uniform velocity profile is enforced with a turbulent intensity of 5%. We set the inlet velocity magnitude so as to achieve a volumetric flow rate corresponding to five air-changes per hour, i.e. ACH = 5. For the room shown in Fig. 1, an inlet velocity of 7.14 m/s corresponds to an ACH = 5 flow rate. The working fluid is air with a density and dynamic viscosity of 1.20 kg/m³ and 1.81×10^{-5} N s/m², respectively. We further note that the mesh independence study was performed in our earlier work [32]. More specifically, we performed simulations with various mesh resolutions, ranging from 4.4 to 7.28 million grid elements. The results based on average velocity indicate that the present grid resolution of 6.27 million elements is adequate.

The numerical domain is initially seeded with one million droplet nuclei that are uniformly but randomly distributed. The radius r of these nuclei ranges from 0.1 to 10 μm (166,667 nuclei per size). The size range of nuclei is chosen such that the smallest (resp. largest) nuclei have a still fluid settling velocity on the order of 1 µm/s (resp. 1 cm/s). This implies that the largest nuclei will deposit on the ground within minutes, while the smallest nuclei, in the absence of ventilation, would remain suspended for days. The main purpose of the simulations is to track these nuclei and identify the paths they take until they are removed from the domain either through the outlet or by depositing on the walls or by settling onto the floor. While the number of nuclei presently considered is far in excess of what would be ejected by a sick individual in a typical room, such a large number is needed to obtain statistically relevant results. The instantaneous threedimensional velocity for a nucleus is affected by its settling velocity and the surrounding air flow. Details on how we resolve nuclei trajectories can be found in [29,32].

3. Pathogen inhalation

The amount of pathogen inhaled by a susceptible individual may be estimated from the well-mixed model [29,31,33,34]. Consider the scenario of a sick person entering a room of volume \mathcal{V} and ejecting virus-laden droplet nuclei at a steady rate of $Q_b n_{so}(r)$ nuclei per second into the room. Here Q_b is the exhalation rate of the sick person (volume per second) and n_{so} is the concentration of fully-desiccated airborne nuclei of radius r in the exhaled air. The well-mixed model assumes that the droplet nuclei are well mixed within the room to result in a time-dependent, but spatially uniform, nuclei concentration n_{wm}^V , which in normalized form can be expressed as [29,31,33,35,36]

$$\hat{n}_{wm}^{V}(t,r) = \frac{n_{wm}^{V}(t,r)}{Q_{b}n_{so}(r)} = \frac{1}{\lambda_{wm}(r)\mathcal{V}} \left[1 - e^{-\lambda_{wm}(r)t} \right] , \qquad (1)$$

where $\lambda_{wm}(r)$ represents the decay rate of nuclei in the room, which in the well-mixed model can be expressed as [31]

$$\lambda_{wm}(r) = \frac{\text{ACH}}{3600} + \frac{V_s(r)}{H} + \lambda_{dep} + \lambda_{da}, \tag{2}$$

where $V_s(r)$, H, λ_{dep} , and λ_{da} represent the size-dependent droplet settling velocity, the room height, the rate of nuclei deposition on the

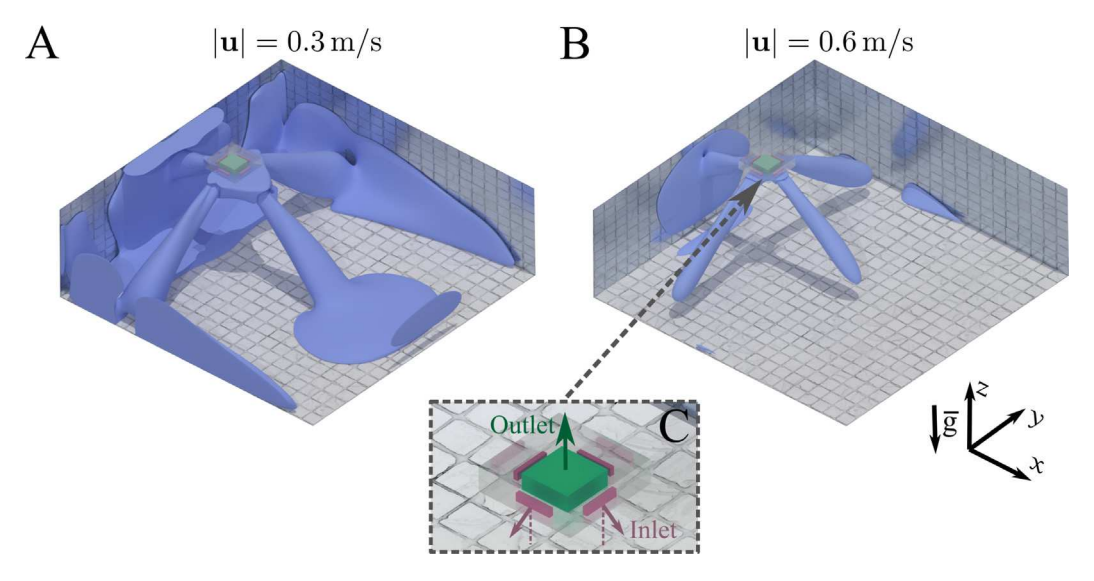


Fig. 1. Iso-surfaces of air flow velocity magnitude for Room 1a for values of (A) 0.3 m/s and (B) 0.6 m/s. (C) Enlarged view of the 4-way cassette AC showing 4 inlets surrounding a square-shaped outlet.

walls, and the exponential rate of viral deactivation, respectively. The viral deactivation rate, λ_{da} , is set at 0.3 h⁻¹ [36,37]. Here ACH is the effective air changes per hour in the room. The four terms on the right hand side correspond to removal by ventilation, gravitational settling on the floor, turbulent deposition on the sidewalls and ceiling, as well as virus deactivation.

The well-mixed model disregards the distance between the source of the nuclei (the sick individual) and the receiving host. According to the well-mixed model the infectious quanta inhaled by the sink is independent of distance from the source. In reality, there are two major departures from the well-mixed model: (i) nuclei require a finite time to disperse from the source to the far corners of the room, and (ii) nuclei ejected from a particular source may not be uniformly distributed in the room, but rather may be on average more readily available in the vicinity of the source. A correction function γ to account for the above two deviations from well-mixedness was recently proposed [29,32,38]. In those studies, γ was obtained as a function of time and the source–sink separation distance d for a particular room configuration (geometry and AC location). For example, a value of $\gamma = 1.5$ implies that nuclei concentration is 50% larger than what is estimated by the well-mixed model, and a value of $\gamma = 0.8$ implies that nuclei concentration is 20% smaller than what is estimated by the well-mixed model. In the vicinity of the source, γ is usually greater than 1, while farther away it is less than 1. Furthermore, in the limit of large time, $\gamma(t,d)$ tends to $\gamma_{\infty}(d)$, which is solely a function of d.

With the correction function, the size-weighted average of normalized concentration of virus-laden nuclei available for inhalation at the sink (integrated over all nuclei sizes) can be expressed in terms of the well-mixed value as [38]

$$\gamma(t,d) \frac{\int_{0}^{r_{c}} \hat{n}_{wm}^{V}(\tau,r)V(r)Q_{b}n_{so}(r)dr}{\int_{0}^{r_{c}} V(r)Q_{b}n_{so}(r)dr}$$
(3)

where the integration is over all nuclei sizes and $V(r)=(4/3)\pi r^3$ is the volume of a droplet nucleus of radius r. Substituting for $\hat{n}_{wm}^V(t,r)$ from Eq. (1), we can see that the amount of virus-laden droplet nuclei at the sink depends only on $\lambda_{wm}(r)$ and $\gamma(t,d)$, apart from the physiological details of the rate at which droplet nuclei are ejected by the source, i.e., $Q_b n_{so}(r)$. In other words, the fluid mechanical details of droplet nuclei dispersal from the source to the sink is entirely now contained in the well-mixed decay rate $\lambda_{wm}(r)$ and the correction function $\gamma(t,d)$. These two quantities will be used to compare the different room configurations studied in this work.

Table 1
Room configuration. Each room can differ from the baseline case (Room 0) through room dimensions, type and location of AC, and the presence of an open window.

Name	Room Dimension (m)	AC type	AC location	Window	ACH
Room 0	$10 \times 10 \times 3.2$	4-way	Ceiling center	No	5
Room 1a	$10 \times 10 \times 3.2$	4-way	Ceiling off-center	No	5
Room 1b	$10 \times 10 \times 3.2$	1-way	Sidewall	No	5
Room 1c	$10 \times 10 \times 3.2$	4-way	Ceiling center	Yes	5
Room 2	$11.8 \times 7.6 \times 2.3$	4-way	Ceiling off-center	No	5

4. Results and discussion

In this section, we will present results for flow and particle nuclei statistics for four different configurations. Each configuration corresponds to a particular room geometry, AC type (1-way vs 4-way cassette) and AC location, as well as the presence of an open side-wall window. The AC units used in the present study are not identical to any particular unit on the market. The wall-mounted unit most closely resembles LG's ARNU12GSJN4 model. On the other hand, the 4-way cassette AC unit most closely resembles a 14 kW, single-vane Variable Refrigerant Flow (VRF) module. We note that aside from the ventilation outlet, only Room 1c possesses an external boundary in the form of a small open window of size comparable to the AC outlet. The window is modeled as a pressure outlet with a corresponding pressure value of 1 atm. The room configurations are summarized in Table 1. By varying the room configurations, we can assess the effect on nuclei statistics. The baseline case to be considered is Room 0, which was the focus of the papers of [29,32].

4.1. Room 1a — asymmetrically-installed 4-way AC

The first modification that we consider to the 8-fold symmetric baseline configuration [29,32] is to shift the location of the AC as shown in Fig. 1A. The AC has been shifted solely along the x-axis by a distance of 2.5 m. The present configuration and that of the baseline case therefore remain identical except for the location of the AC. In Fig. 1, we show iso-surfaces of flow velocity magnitude of 0.3 m/s (panel A) and 0.6 m/s (panel B). In panel C, we show an enlarged view of the AC unit. The air velocity magnitude in the majority of the room is on the order of 0.1 m/s, however in the direct path of the inlet jets, the velocity can be substantially higher as observed from Fig. 2.

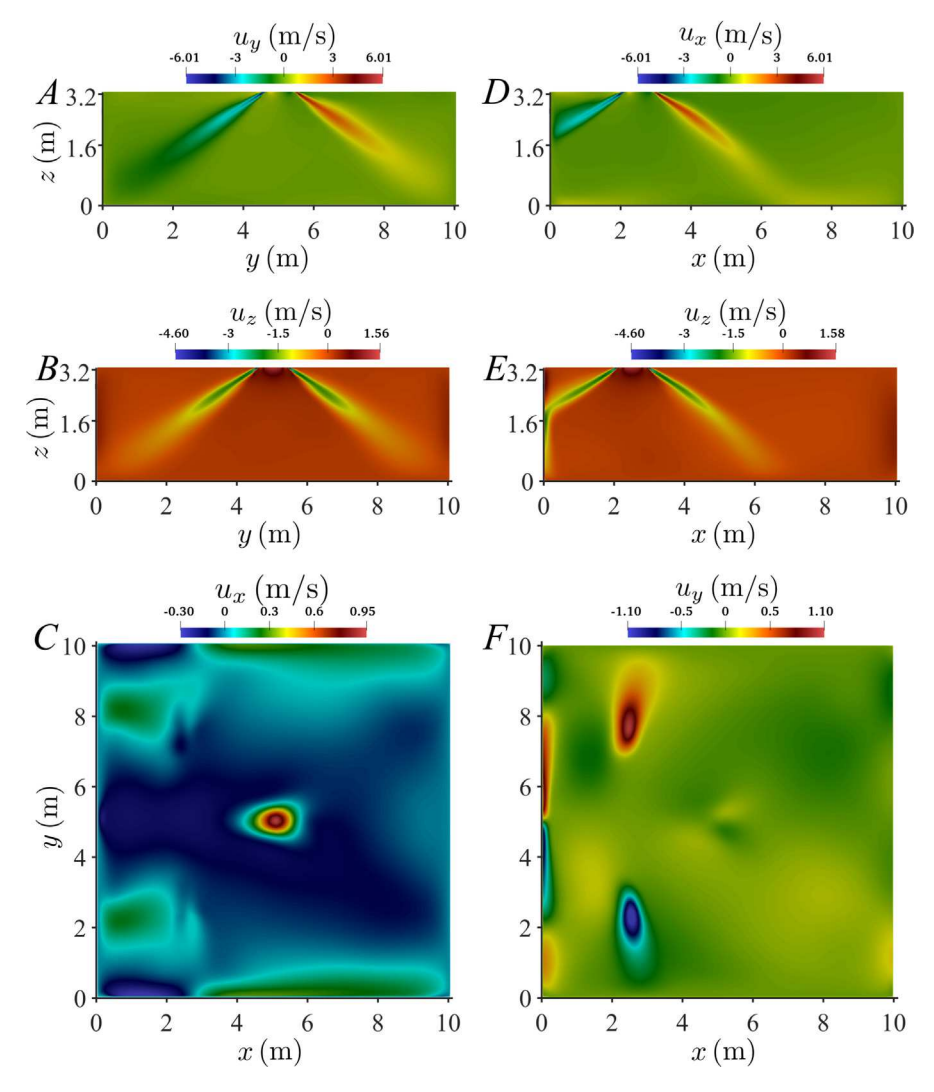


Fig. 2. Velocity iso-contour for Room 1a (AC shifted) (A) y-component of velocity at plane x = 2.5 m. (B) z-component of velocity at plane x = 2.5 m. (C) x-component of velocity at plane y = 5 m. (E) z-component of velocity at plane y = 5 m. (F) y-component of velocity at plane z = 1.6 m.

Figs. 2A and 2B show the velocity components u_y and u_z , plotted in the x=2.5 m plane (i.e. the plane bisecting the AC along the x-axis). Panels D and E show u_x and u_z plotted in the y=5 m plane (i.e. the plane bisecting the AC along the y-axis). Panels C and F show the x and y components of velocity in the z=1.6 m plane (i.e. midway between the floor and the ceiling). Panels A, B, C, and F highlight the symmetry of the flow about the y=5 m-plane. The velocity magnitude is observed to be on the order of 0.1 m/s in the vast majority. It is noticeably larger near the paths of the inlet jets. We further note that while the color-bar indicates a range from -6.01 to 6.01 m/s, such high values are only present very close to the inlet. These air velocities quickly decay to attain values of around 1 m/s within the direct path of the jet halfway between the floor and the ceiling. The air velocities remain around 0.1 m/s for the overwhelming majority of the room.

The particle statistics for Room 1a are shown in Fig. 3. In panel A, we plot the exponential decay rate λ for the six nuclei sizes as a function of the nuclei radius r. The cross symbol corresponds to the well-mixed theory of Bazant & Bush [31], whereas the circle and square symbols correspond to the LES results for Room 0 and the RANS results for Room 1a. The Greek symbol λ represents the rate at which nuclei are removed from the room. Nuclei removal occurs through the outlet via ventilation, by turbulent deposition on the walls, or by gravitational settling on the floors [29,32,38]. The ventilation outlet is the dominant form of removal for smaller nuclei, whereas gravitational settling is

the dominant form for larger nuclei. Nuclei removed via turbulent deposition usually amounts to only a few percent of the total amount of nuclei removed.

It must be emphasized that Panel A is the result of room-averaged statistics. The good agreement between the RANS results and theory validates the appropriateness of the well-mixed assumption when averaged over the entire room. Put simply, when the exact location of the source is uncertain (which is common), it is suitable to average across all potential source positions within the room. Additionally, the resulting average nuclei concentration remains well-distributed within the room.

However, when applied to a particular source location within the room, the well-mixed model must assume that the nuclei once ejected following an expiratory event are instantaneously and uniformly distributed within the room and are available at equal probability at any location irrespective of the distance from the source. Clearly, nuclei require a finite time to disperse and are likely to be observed closer to the source than farther away. This departure from well-mixedness can be correctly described only with a two-point statistics that takes into account the location of the sink with respect to the source, instead of the single-point statistics contained in the well-mixed model. As discussed in Section 2, this two-point statistics that accounts for departure from room-averaged concentration is represented by the correction function $\gamma(t,d)$. In Fig. 3B we plot the long-time value of the correction function

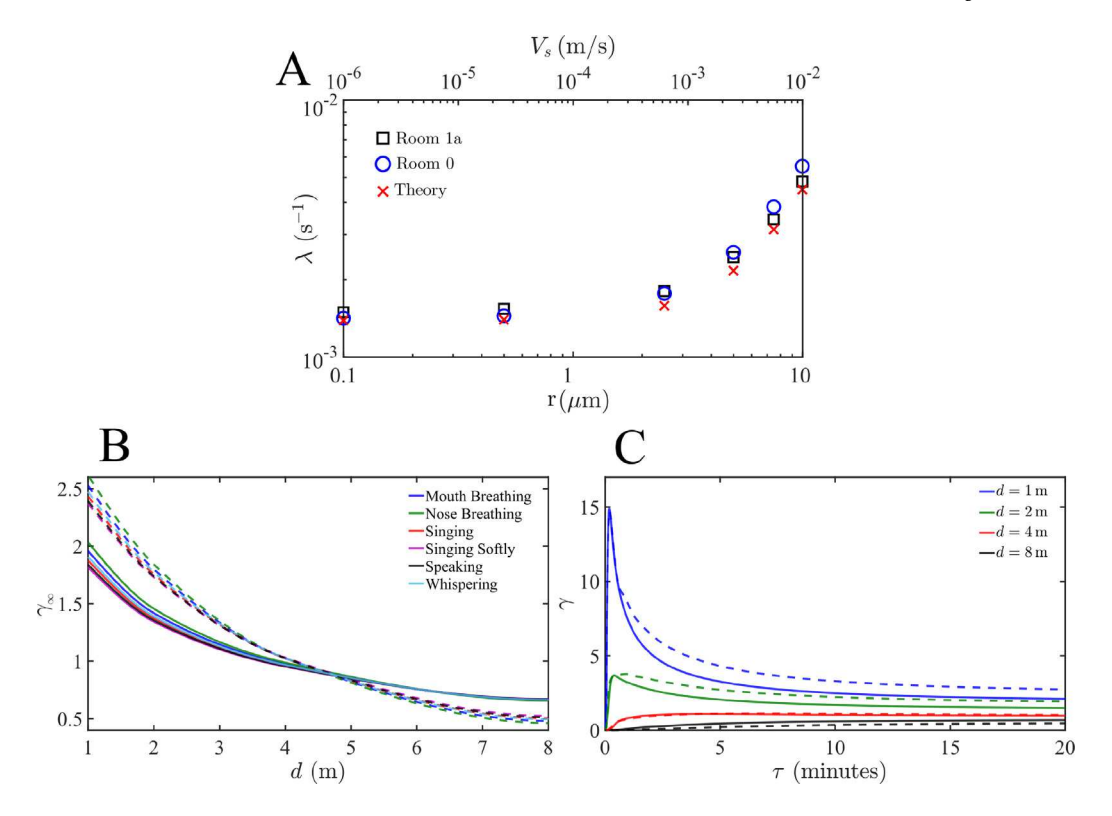


Fig. 3. (A) Exponential rate λ vs nuclei radius r and the corresponding settling velocity V_s from the well-mixed theory of Bazant & Bush [31], the LES simulation results of Room 0, and the RANS of Room 1a. (B) The steady-state correction function, which depends on the source-to-sink distance, for different expiratory activities from Room 1a (solid curves) and Room 0 (dashed curves). (C) The time-dependent correction function for γ as a function of exposure time τ for separation distances of d = Im (blue), 2 m (green), 4 m (red), and 8 m (black) from Room 1a (solid curves) and Room 0 (dashed curves). (For interpretation of the references to color in this figure legend, the reader is referred to the web version of this article.)

 γ_{∞} versus d for Room 0 (dashed curves) and Room 1a (solid curves) and for various types of expiratory events (breathing, singing, etc.). We note that the ejected droplet spectra for different expiratory activities were obtained from the experimental work of [34]. A value of $\gamma_{\infty}=2$ for d=1 m, for example, implies that on average, and after sufficiently long time, nuclei concentration is twice the value predicted by the well-mixed model at locations that are d=1 m away from the source. Similarly a value of $\gamma_{\infty}=0.5$ for d=8 m, for example, implies that on average and after sufficiently long time, nuclei concentration is half the value predicted by the well-mixed model at locations that are d=8 m away from the source.

However, the concentration at any finite source-sink separation needs a finite travel time before it starts to build up. The correction function is in fact time-dependent as shown in Fig. 3C, where for shorter separation distances below 2 m, we observe the existence of a peak, where nuclei concentration is temporarily far in excess (up to 15 times) of the prediction from the well-mixed model. Such a peak does not exist for larger separations, where the correction function monotonically increases to its long-term or steady state value γ_{∞} . The existence of the peaks, and consequently their absence, can be rationalized as follows. Consider the d = 1 m curve, which represent the scenario where individuals are seated 1 m apart. As nuclei are being ejected, they require a finite time to propagate away from the source. During this short time-span, the well-mixed model which assumes instantaneous mixing over the entire room, will greatly underestimate the actual nuclei concentration at short separation distances. Similarly for d = 8 m, the well-mixed model will largely overestimate the concentration at early times. This is manifested by the near-zero value of γ for small values of τ in Fig. 3C.

Panels A, B, and C of Fig. 3 provide a quantitative measure to assess how AC location within the room affects nuclei dispersal and concentration within the room. In the subsequent sections, we will present similar plots to investigate the effects of room size, AC type, and

the presence of open windows on nuclei distribution within the room and departure from well-mixedness. For the configuration presently considered, i.e. Room 1a, we find γ_{∞} to be smaller for shorter separations d and correspondingly larger for larger separations. That is, for Room 1a, the effect of shifting the AC from the center of the ceiling tends, on average and compared to the baseline case Room 0, to increase the likelihood of particles to propagate over longer distances, and consequently reduce the likelihood of observing them at shorter separation distances. In other words, the shifting of the 4-way cassette AC from the center of the room to one side, results in more uniform distribution, from the perspective of the two-point statistics. We emphasize that at the level of room-averaged single-point statistics both AC configurations are well-mixed and are in agreement with the well-mixed theory. The difference appears only in the twopoint statistics contained in the correction function γ . We note here that the time duration of the simulations, which is on the order of 20 min, is chosen to be long enough to capture the trend in the temporal evolution of the correction function γ . It is consistent with the duration used in previous studies for ACH = 5[29,32,38].

The fact that the nuclei concentration in the central AC configuration is less uniform in two-point statistics is somewhat counter intuitive. The explanation for the above behavior can be deduced from Figs. 2D and 2E. With the shifting of the AC to one side, we find the jet along the positive *x*-axis to have a relatively unobstructed path, which increases the likelihood of nuclei to cover larger distances in excess of 6 or 7 m. As a result, many more source/sink combinations of more than 5 m separation have a direct path for nuclei transport. For the baseline case Room 0, nuclei traveling larger distances such as 8 m, would have to likely maneuver around the inlet jet paths to reach their destination. In other words, for the baseline case, the inlet jets act to separate the room into segmented zones and somewhat limit the propagation of nuclei over larger distances than 5 m. Once the AC is shifted to one side, this obstruction is partially relaxed.

9

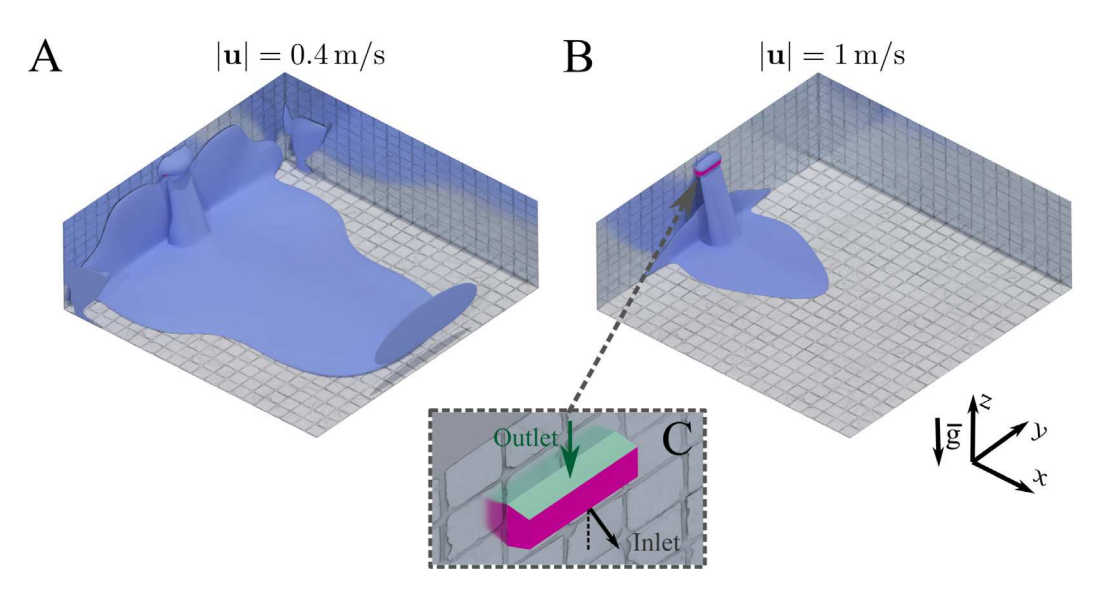


Fig. 4. Iso-surfaces of air flow velocity magnitude for Room 1b for values of (A) 0.4 m/s and (B) 1 m/s. (C) Enlarged view of the wall-mounted AC, which is comprised of a single inlet and a single outlet.

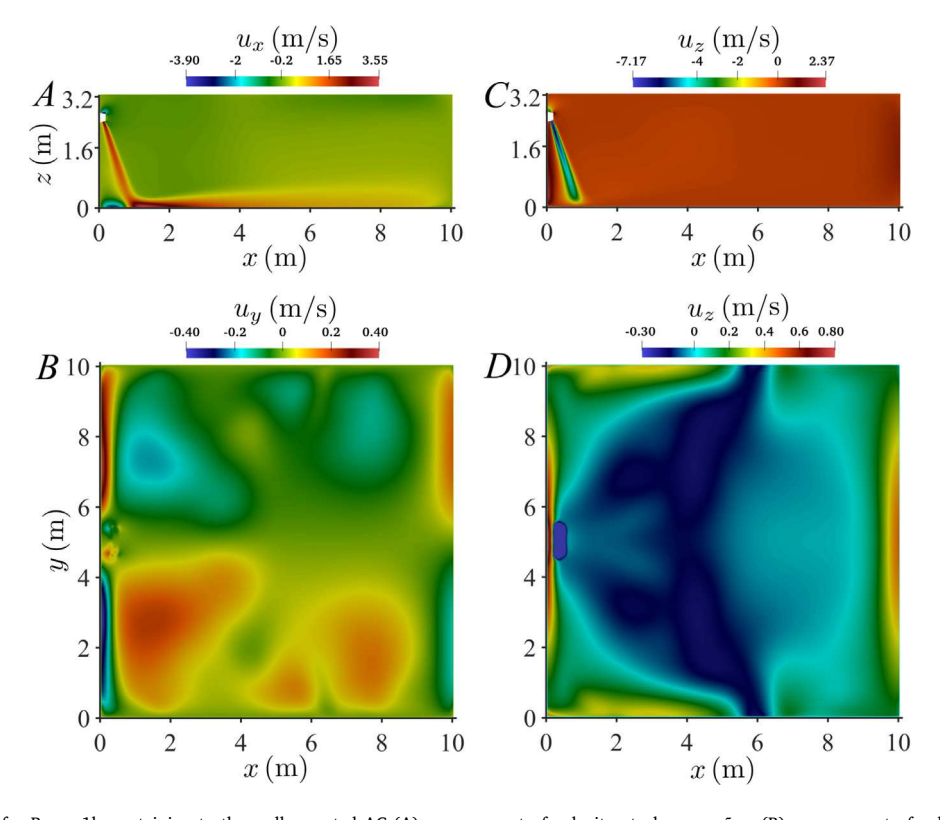


Fig. 5. Velocity iso-contour for Room 1b, pertaining to the wall-mounted AC (A) x-component of velocity at plane $y = 5 \,\mathrm{m}$. (B) y-component of velocity at plane $z = 1.6 \,\mathrm{m}$. (C) z-component of velocity at plane $y = 5 \,\mathrm{m}$. (D) z-component of velocity at plane $z = 1.6 \,\mathrm{m}$.

4.2. Room 1b — wall-mounted AC

The second configuration to be considered is Room 1b. This room differs from the baseline case Room 0 by the type of the AC (1-way vs 4-way cassette) and its placement on a sidewall. The same air flow rate is however delivered, which results in the same value of ACH = 5. An iso-surface of velocity magnitude is shown in Fig. 4. The inlet is inclined towards the floor making an angle of 73° with the ceiling. The flow impinges on the floor and spreads primarily along the x-axis with

the maximum velocity remaining close to the floor. The inlet jet can be seen to penetrate all the way towards the other end of the room as seen from Fig. 4. This is confirmed in Fig. 5, specifically frames A and D. In Frame A, we plot the x-component of velocity, where the incoming jet is observed to remain in the vicinity of the floor for the entire length of the room, before rising on the x=10 m wall (the wall opposite to the placement of the AC) as observed from Frame D. This large flow cell spanning the entire length of the room should be contrasted with the scenario where the room is divided into left and right sections along

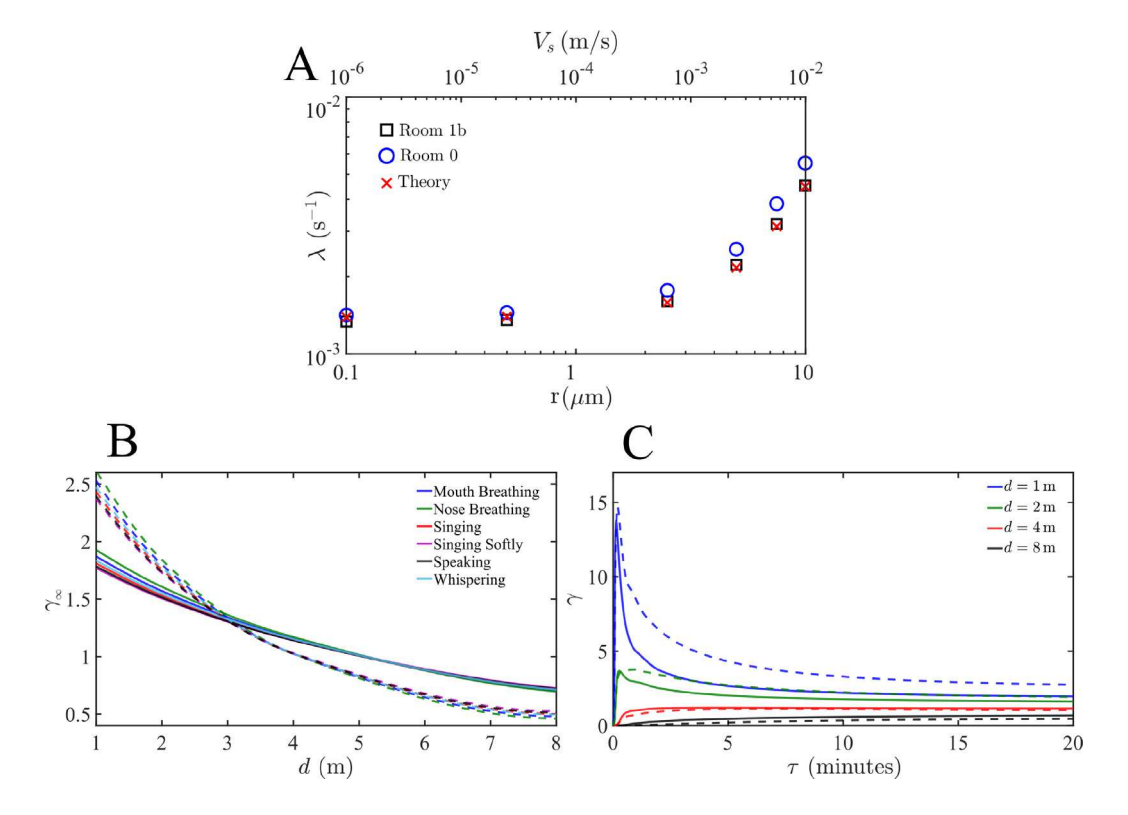


Fig. 6. (A) Exponential rate λ vs nuclei radius r and the corresponding settling velocity V_r from the well-mixed theory of Bazant & Bush [31] and the LES results of Room 0 and the RANS of Room 1b. (B) The steady-state correction function, which depends on the source-to-sink distance, for different expiratory activities from Room 1b (solid curves) and Room 0 (dashed curves). (C) The time-dependent correction function for γ as a function of exposure time τ for separation distances of d=1m (blue), 2 m (green), 4 m (red), and 8 m (black) from Room 1b (solid curves) and Room 0 (dashed curves). (For interpretation of the references to color in this figure legend, the reader is referred to the web version of this article.)

the x-axis (similarly along the y-axis) in the reference case of Room 0. Consequently, Room 1b and Room 0 can be viewed as two extreme points representing a continuous range of AC placements, with Room 1a falling in between them. Regardless of the configuration, all three cases maintain symmetry in the flow relative to the plane y = 5 m.

The various frames in Fig. 5 indicate that the flow pattern for Room 1b is complex. For example, in Frame B, we observe y-component of velocity contours indicative of additional recirculation regions. More specifically, near the x=0 wall, the wall on which the AC is placed, we find a thin region of flow oriented towards the nearest sidewall with a slower return flow occupying a relatively larger region. This return flow extends roughly from the x=1 m to the x=3 m region in Frame B. Other such regions can also be observed in Frame B near the x=10 m wall

From Fig. 6A, we find the room-averaged nuclei statistics to match the baseline case Room 0 as well as the well-mixed theory especially for small-sized nuclei. This agreement is expected since nuclei concentration will be well-mixed in the room at the level of single-point statistics. Fig. 6B shows a similar trend to Fig. 3B, more specifically that, compared to the baseline case, the shifting of the AC unit reduces (resp. increases) the likelihood of observing nuclei at short (resp. large) separation distances. In other words, once nuclei are continuously ejected at a particular location in the room, then on average and over long time, they are more likely to propagate over larger distances for the configuration of Room 1b than they are for the baseline configuration of Room 0. Here we argue again that this behavior is due to nuclei having a relatively unobstructed path as they propagate from one side of the room to the other. The multi-cellular nature of the mean flow that prevents nuclei from having a direct pathway over large separation distances in the baseline case is avoided with the shifting of the inlet jets to one side of the room.

4.3. Room 1c — symmetric 4-way AC with open window

We now assess the effect of an open window. The open window provides another venue for nuclei to exit the room. The window has dimensions of 20 cm \times 100 cm and is placed at the center of one of the sidewalls. The size of the window is chosen to be small and comparable to the size of the AC outlet, having a surface area of 0.36 m², and thus serves only as an example to study the effect of including another air outlet. For the present setup, the removal rate from the window for the smallest nuclei size is approximately 55% of the removal rate through the outlet. For the configuration considered, as shown in Fig. 7, the overall flow is only mildly affected by the presence of the window except for the region in its immediate vicinity. Furthermore, the nuclei statistics are observed to remain fairly unchanged as compared to the baseline case Room 0 and therefore not repeated here. This applies to the room-averaged statistics as well as to the time- and space-dependent correction function γ .

If the window dimensions were larger, or if additional windows were installed, the detailed results of such an arrangement can be expected to differ and therefore will require additional simulations. It can however be conjectured that although the flow may be different than the baseline case, as long as the ACH remains the same, the room averaged nuclei statistics may not be affected. The effect of larger windows on two-point statistics and the correction function γ needs to be further investigated. Here, with the addition of another pressure outlet in the form of an open window, we find the nuclei to remain well-mixed. The statistics also suggest that a proportionate amount of nuclei exit the room through the window compared to the AC outlet. The behavior of the correction function γ remains practically identical to the baseline case. This clearly highlights the insensitivity of one and

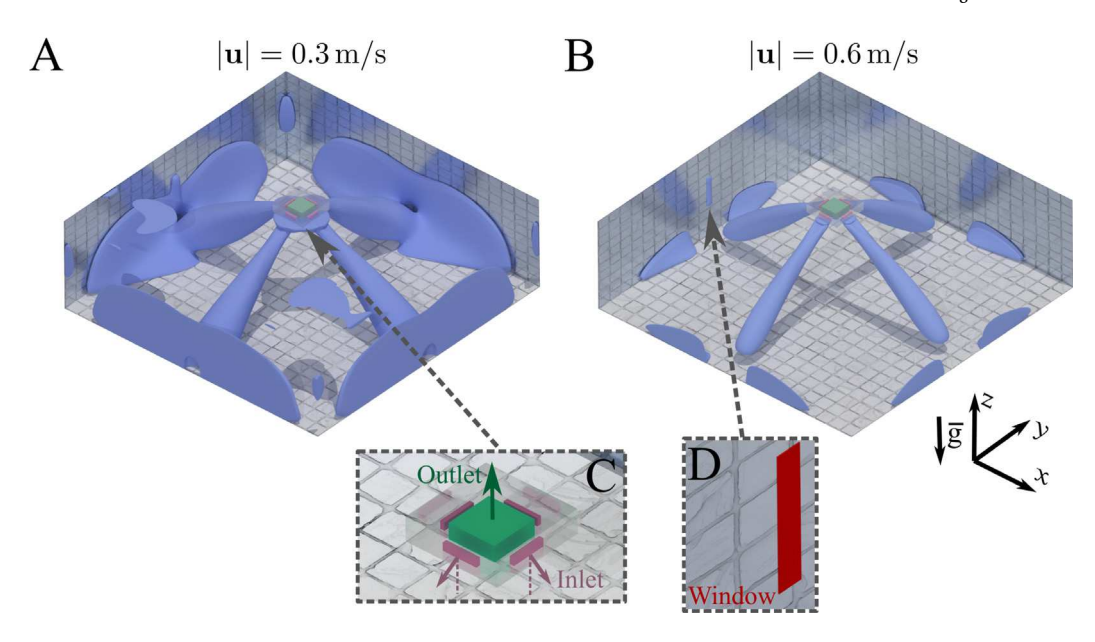


Fig. 7. Iso-surfaces of air flow velocity magnitude for Room 1c for values of (A) 0.3 m/s and (B) 0.6 m/s. (C) Enlarged view of the 4-way cassette AC showing 4 inlets surrounding a square-shaped outlet. (D) Enlarged view of the window.

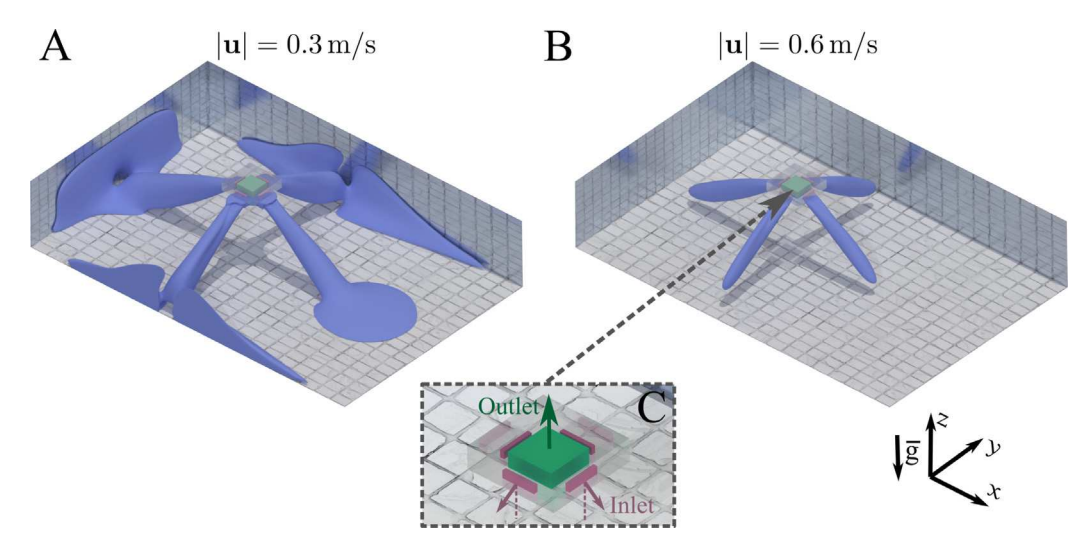


Fig. 8. Iso-surfaces of air flow velocity magnitude for Room 2 for values of (A) 0.3 m/s and (B) 0.6 m/s. (C) Enlarged view of the 4-way cassette AC showing 4 inlets surrounding a square-shaped outlet.

two-point nuclei statistics to the presence of a window as long as the ACH remains the same.

We further note that our purpose here is to assess the effect of an open window on pathogen removal in the absence of any heat load. Clearly, this is by no means a representation of many possible scenarios including heating/cooling load. In such cases, the natural convection due to the temperature variations may significantly modify the flow field. Additionally, from a practical point of view, and since the data was shown to collapse for different values of ACH, the results of this study may be used in the case of relatively high ACH, where the effect of natural convection is small.

4.4. Room 2 — 4-way AC in a 2-way symmetric room

The configuration for Room 2 differs from the baseline case by the shape and size of the room as well as by the asymmetric location of the AC. As shown in Fig. 8, Room 2 has a rectangular floor area with dimensions of 11.8 m \times 7.6 m. The height of the room is 2.3 m, which is smaller than that of the baseline case (i.e. 3.2 m). The 4-way cassette

AC is located on the ceiling and centered at x=5 m and y=3.8 m (see Fig. 8). For ACH = 5, the volumetric flow rate for Room 2 is smaller than the other cases considered since the volume of Room 2 is approximately 35% smaller than that of the baseline case Room 0 as well as Room 1. Also, since the dimensions of the 4-way AC are identical to the baseline case, it follows that the inlet jet speed is also reduced by about 35% to a value of 4.6 m/s. The 3D flow structure shown in Fig. 8 remains similar to the baseline case except that the inlet jets on the short sides now impinge on the sidewalls. We still observe the tear drop shape for the jets in the z=1.15 m plane. Clearly, the flow is affected by the asymmetric geometry of the room with the y-aligned jets drifting in the positive x direction as they near the sidewalls.

In Fig. 9A we plot the decay rate λ versus nuclei radius r and settling velocity V_s in the inset. Since the dimensions of Room 2 differ from the baseline case, and more specifically, since the ceiling height is different, the well-mixed theory of Bazant & Bush [31] will predict an enhanced decay rate for the same nuclei size (i.e. the black symbols, which correspond to Room 2 are consistently higher then their red counterparts, which correspond to the baseline case Room 0). This

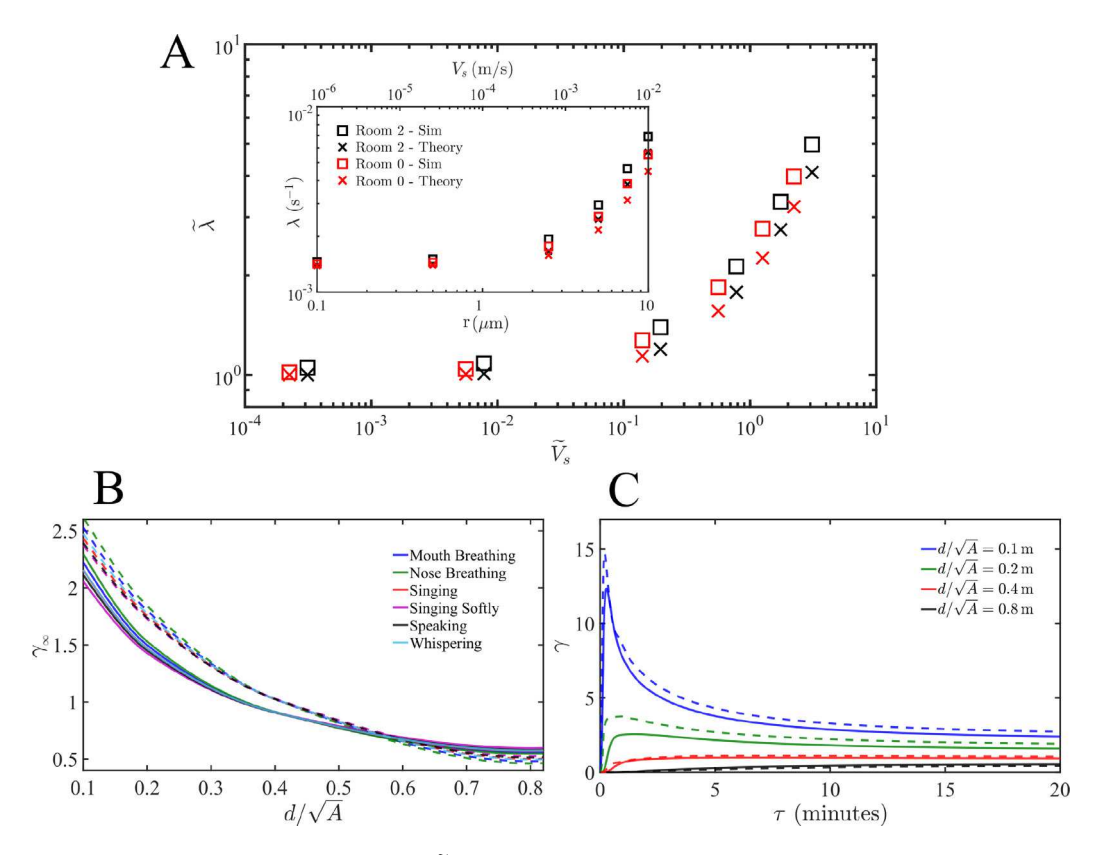


Fig. 9. (A) ACH-scaled exponential rate $\tilde{\lambda}$ vs ACH-scaled settling velocity \tilde{V}_s . Inset: Dimensional λ vs V_s . (B) Steady-state correction function as a function of source-to-sink scaled distance d/\sqrt{A} for different expiratory activities for ACH = 5 from Room 2 (solid curves) and Room 0 (dashed curves). (C) Time-dependent correction function for ACH = 5 as a function of exposure time for scaled separation distances of d/\sqrt{A} = 0.1 (blue), 0.2 (green), 0.4 (red), and 0.8 (black) from Room 2 (solid curves) and Room 0 (dashed curves). (For interpretation of the references to color in this figure legend, the reader is referred to the web version of this article.)

behavior is consistent with the simulation results and is due to the enhanced gravitational settling. For the same nuclei size, the settling velocity is unchanged, however the distance that nuclei must cover to settle on the bottom floor is reduced from 3.2 m in the baseline case to 2.3 m in Room 2. This translates into nuclei remaining suspended for shorter times and consequently a higher decay rate λ . Nonetheless, when λ and V_s are normalized by ACH as the inverse time scale and room height H as the length scale, then we observe the nondimensional decay rates of nuclei from both rooms to collapse onto a single curve [29,32,38]. A plot of the dimensionless decay rate ($\tilde{\lambda}$ = $3600\lambda/ACH$) vs dimensionless settling velocity \widetilde{V}_s is shown in the main frame of Fig. 9A. Fig. 9A suggests the room remains well-mixed, and the room-averaged decay rate can be well-represented by the well-mixed theory. Similarly, the values of γ_{∞} are independent of ACH, and the values of γ can be made to be independent of ACH by stretching (for larger values of ACH) or contracting (for smaller values of ACH) the time axis through multiplication by ACH.

In Fig. 9B, we plot the long-time, steady-state correction function γ_{∞} vs separation distance d normalized by the square root of the room cross-section A. This scaling is necessary for a fair comparison [38]. From Fig. 9B, we observe γ_{∞} is smaller (resp. larger) at short (resp. long) normalized separation distances when compared to the baseline Room 0 configuration. This trend in γ_{∞} is consistent with what we observed for Rooms 1a and 1c. Namely, that nuclei can travel larger distances without having to maneuver around impinging jets.

In Fig. 9C, we plot the time-dependent correction function γ versus exposure time τ for four scaled separation distances (d/\sqrt{A}) , namely 0.1, 0.2, 0.4, and 0.8. We observe a similar trend compared to the baseline case. For short separation distances, both cases exhibit the peaks for early exposure times. Nonetheless, the values from the baseline case remain higher. In fact, when γ_{∞} for the baseline case is larger than that for Room 2, we find the value of γ to be consistently larger, and

vice versa. Additionally, for the larger separation distances, γ increases monotonically towards γ_∞ as observed in all other cases.

5. Conclusions

Airborne contagion within indoor spaces depends on many factors such as viral infectivity, the overall health of the receiving host, as well as the local concentration of virus-containing droplet nuclei inhaled by the receiving host. The latter is a fluid dynamics property that depends on several factors including room geometry, the magnitude of ventilation measured in terms of ACH, AC location within the room, and the separation distance between the infected person and the receiving host. The time evolution of the virus-laden nuclei concentration following the arrival of a sick person into a room may be estimated from the well-mixed model [31]. Such a room-averaged estimate however cannot account for the important effect of spatial variation, and as such predicts the same risk of contagion irrespective of the separation distance between the sick individual and the receiving host. I.e. it makes no difference whether individuals are 2 m or 20 m apart. A correction function that accurately accounts for this important effect has recently been developed and tested [29,32]. For a specific room with a particular AC setup, the ability of the well-mixed model to accurately predict the inhaled viral quanta was demonstrated only when used in conjunction with the correction function [29,32]. The purpose of this paper is to assess the effect of room geometry, AC location, and the presence of an open window on the appropriateness of the well-mixed model along with the correction function γ .

To that end, we considered two room geometries with different AC types and locations, with one of the rooms containing an open window. The main conclusions will be separated into those pertaining to the prediction of single-point, room-averaged concentration statistics and those pertaining to two-point concentration statistics that depends

on source-sink separation. In the context of mechanical ventilation, pathogens remain well-mixed within the room, only when averaged over all possible source locations. This average concentration depends only on the balance between the expiratory event and the decay rate of pathogens by the overall ACH. Consistent with previous findings [39], this well-mixed source-averaged concentration is observed to be insensitive to details such as room geometry, AC placement, or the presence of an open window. It is primarily a function of the balance between the production rate of droplet nuclei by the source and its removal rate λ determined by ACH, settling velocity, and deactivation. Furthermore, this insensitive room-averaged nuclei concentration is quite accurately given by the well-mixed model. In other words, room-averaged nuclei concentration can be well predicted with the production rate and the well-mixed decay rate λ_{wm} as given in (1). The effects of air recycling back into the room and the level of filtration of the recycled air on the room-averaged concentration can be easily accounted for with an effective ACH [38]. In fact, most office buildings in the US, exhaust the return air to a plenum, where the air is mixed with outdoor air and re-delivered into the office rooms [40]. Studies that consider the effect of filtration [38,40-42] do show that the level of pathogens increases as filtration efficiency decreases, and that recycled pathogens tend to be more well-mixed compared to pathogens ejected by a stationary person in the room. In the current study, we only took into account the scenario in which the air entering the room is completely clean, which can be achieved by perfectly filtering recycled air or by bringing fresh air in from the outside. This situation is comparable to the use of an AC unit with a HEPA filter, which removes over 99.9% of pathogens. Furthermore, the present setup considered the case where the filters are positioned at the level of the air handling unit, which is in front of the air-conditioning fan. We observe the AC location within the room to affect the behavior of the spatio-temporal correction function γ and its long time asymptotic value γ_{∞} . In particular, when the AC location is such that the inlet jets go unhindered for the entire length of the room, then γ_{∞} will decrease towards unity for small separation distances and correspondingly increase towards unity for large d. Such a scenario occurs for a wall-mounted AC as opposed to a ceiling-mounted AC installed at the center of the room. Since γ 's departure from unity represents a correction to the well-mixed nuclei concentration, it can be concluded that a one-cell, room-wide circulation induced by a wallmounted AC decreases the dependence of nuclei concentration on the source-sink separation distance. This behavior is due to the fact that nuclei are able to travel larger distances unobstructed in the one-cell, room-wide circulation generated from a wall-mounted AC. This effect of AC placement on γ_{∞} can be as large as 50%. This implies that, on average, it is relatively safer to be seated well-apart in a room with the AC located at the center of the ceiling than in a room with a wall-mounted AC.

We observe that the size of the room can be properly accounted for in the correction function by scaling the source-sink separation distance d by the characteristic length of the room. In other words, the correction to the well-mixed concentration only depends on the separation distance d scaled by the room size. We also observe the room-averaged nuclei concentration and the correction function to be independent of the presence of an open window in one of the walls, and thus supporting the view that the present results are applicable even in the case of air leakage, as long as the total air flow in and out of the room is captured by the room ACH. Furthermore, the type of expiratory activity, i.e. breathing, singing, speaking, etc., does not have any noticeable effect on $\gamma(t,d)$. Nor does the strength of ventilation, quantified as air changes per hour (ACH), affect the value of γ , when time is properly scaled by ACH. In conclusion, with the results of the present work summarized in terms of λ_{nm} and γ , we are able to accurately predict the virus-laden nuclei concentration in indoor spaces for a wide range of room size/shape, AC placement, as well as recycling and filtration characteristics of the AC.

As far as comfort of occupants is concerned, a key parallel metric along with concentration of viral matter is the mean age of air. In the present simulations, and due to the turbulent nature of the flow, the incoming air through the vents is well-mixed in the room. This is confirmed by the exponential rate λ of the sub-micron size nuclei that follow faithfully the decay rate predicted by the well-mixed model. As such, the present ACH value of 5 can be used to infer the mean age of air to be $\bar{\tau}=3600/\text{ACH}=720$ s. Furthermore, aside from the path of inlet jets, we observe the air velocities in the room to be on the order of 0.1 m/s for the vast majority of the indoor space. According to ASHRAE Standard 55 [43], the recommended air speed for thermal comfort in a sedentary environment is typically in the range of 0.1 to 0.2 m/s. However, it is important to note that these values are general guidelines, and individual preferences can vary. Some people may find slightly higher or lower air speeds to be more comfortable.

Finally we note that in the present study, we have ignored the effect of thermal loads due to occupants, electronic equipment, or ambient conditions. As such, we have ignored the resulting flow due to natural convection, which may be significant.

CRediT authorship contribution statement

K. Choudhary: Writing – original draft, Visualization, Validation, Software, Formal analysis, Conceptualization. K.A. Krishnaprasad: Visualization, Validation, Conceptualization. N. Zgheib: Writing – review & editing, Supervision, Conceptualization. M.Y. Ha: Supervision, Resources, Funding acquisition, Conceptualization. S. Balachandar: Writing – review & editing, Supervision, Methodology, Funding acquisition, Conceptualization.

Declaration of competing interest

The authors declare that they have no known competing financial interests or personal relationships that could have appeared to influence the work reported in this paper.

Data availability

Data will be made available on request.

Acknowledgments

We gratefully acknowledge support from The National Science Foundation (EAGER Grant no. 2134083), LG Electronics (Grant no. C2021017165), U.S. Department of Energy NNSA MSIPP Program (Award No. DE-NA0004003), and University of Florida Informatics Institute, United States.

References

- K. Sun, Q. Zhao, Z. Zhang, X. Hu, Indoor occupancy measurement by the fusion of motion detection and static estimation, Energy Build. 254 (2022) 111593.
- [2] M. Qian, J. Jiang, COVID-19 and social distancing, J. Public Health (2020) 1-3.
- [3] J.A. Lewnard, N.C. Lo, Scientific and ethical basis for social-distancing interventions against COVID-19, Lancet Infect. Dis. 20 (6) (2020) 631–633.
- [4] L. Thunström, S.C. Newbold, D. Finnoff, M. Ashworth, J.F. Shogren, The benefits and costs of using social distancing to flatten the curve for COVID-19, J. Benefit-Cost Anal. 11 (2) (2020) 179–195.
- [5] M. Gil-Baez, J. Lizana, J.B. Villanueva, M. Molina-Huelva, A. Serrano-Jimenez, R. Chacartegui, Natural ventilation in classrooms for healthy schools in the COVID era in Mediterranean climate, Build. Environ. 206 (2021) 108345.
- [6] N. Ghaddar, K. Ghali, Ten questions concerning the paradox of minimizing airborne transmission of infectious aerosols in densely occupied spaces via sustainable ventilation and other strategies in hot and humid climates, Build. Environ. 214 (2022) 108901.
- [7] E. Katramiz, N. Ghaddar, K. Ghali, Novel personalized chair-ventilation design integrated with displacement ventilation for cross-contamination mitigation in classrooms, Build. Environ. 213 (2022) 108885.

- [8] A. Foster, M. Kinzel, Estimating COVID-19 exposure in a classroom setting: A comparison between mathematical and numerical models, Phys. Fluids 33 (2) (2021).
- [9] H. Qian, Y. Li, P.V. Nielsen, X. Huang, Spatial distribution of infection risk of SARS transmission in a hospital ward. Build. Environ. 44 (8) (2009) 1651–1658.
- [10] B.J. Schimmoller, N.S. Trovão, M. Isbell, C. Goel, B.F. Heck, T.C. Archer, K.D. Cardinal, N.B. Naik, S. Dutta, A. Rohr Daniel, et al., COVID-19 exposure assessment tool (CEAT): Exposure quantification based on ventilation, infection prevalence, group characteristics, and behavior, Sci. Adv. 8 (39) (2022) eabq0593.
- [11] R. Mittal, R. Ni, J.-H. Seo, The flow physics of COVID-19, J. Fluid Mech. 894 (2020) F2.
- [12] K. Randall, E.T. Ewing, L.C. Marr, J. Jimenez, L. Bourouiba, How did we get here: What are droplets and aerosols and how far do they go? A historical perspective on the transmission of respiratory infectious diseases, Interface Focus 11 (6) (2021) 20210049.
- [13] S. Balachandar, S. Zaleski, A. Soldati, G. Ahmadi, L. Bourouiba, Host-to-host airborne transmission as a multiphase flow problem for science-based social distance guidelines, Int. J. Multiph. Flow. 132 (2020) 103439.
- [14] L. Bourouiba, E. Dehandschoewercker, J.W. Bush, Violent expiratory events: On coughing and sneezing, J. Fluid Mech. 745 (2014) 537–563.
- [15] K. Liu, M. Allahyari, J. Salinas, N. Zgheib, S. Balachandar, Investigation of theoretical scaling laws using large eddy simulations for airborne spreading of viral contagion from sneezing and coughing, Phys. Fluids 33 (6) (2021).
- [16] K. Liu, M. Allahyari, J.S. Salinas, N. Zgheib, S. Balachandar, Peering inside a cough or sneeze to explain enhanced airborne transmission under dry weather, Sci. Rep. 11 (1) (2021) 9826.
- [17] A. Fabregat, F. Gisbert, A. Vernet, J.A. Ferré, K. Mittal, S. Dutta, J. Pallarès, Direct numerical simulation of turbulent dispersion of evaporative aerosol clouds produced by an intense expiratory event, Phys. Fluids 33 (3) (2021).
- [18] B. Stiehl, R. Shrestha, S. Schroeder, J. Delgado, A. Bazzi, J. Reyes, M. Kinzel, K. Ahmed, The effect of relative air humidity on the evaporation timescales of a human sneeze, AIP Adv. 12 (7) (2022).
- [19] T. Peters, A. Halleran, How our homes impact our health: Using a COVID-19 informed approach to examine urban apartment housing, Archnet-IJAR: Int. J. Archit. Res. 15 (1) (2021) 10–27.
- [20] A.M. Hassan, N.A. Megahed, COVID-19 and urban spaces: A new integrated CFD approach for public health opportunities, Build. Environ. 204 (2021) 108131.
- [21] M. Awada, B. Becerik-Gerber, S. Hoque, Z. O'Neill, G. Pedrielli, J. Wen, T. Wu, Ten questions concerning occupant health in buildings during normal operations and extreme events including the COVID-19 pandemic, Build. Environ. 188 (2021) 107480.
- [22] A.K. Melikov, COVID-19: Reduction of airborne transmission needs paradigm shift in ventilation, Build. Environ. 186 (2020) 107336.
- [23] B. Li, W. Cai, A novel CO2-based demand-controlled ventilation strategy to limit the spread of COVID-19 in the indoor environment, Build. Environ. 219 (2022) 109232.
- [24] T. Hu, Y. Ji, F. Fei, M. Zhu, T. Jin, P. Xue, N. Zhang, Optimization of COVID-19 prevention and control with low building energy consumption, Build. Environ. 219 (2022) 109233.
- [25] F. Memarzadeh, W. Xu, Role of air changes per hour (ACH) in possible transmission of airborne infections, in: Building Simulation, Vol. 5, Springer, 2012, pp. 15–28.
- [26] G.H. Downing, Y. Hardalupas, J. Archer, H.E. Symons, U.B. Baloglu, D. Schien, B.R. Bzdek, J.P. Reid, Computational and experimental study of aerosol dispersion in a ventilated room, Aerosol Sci. Technol. 57 (1) (2022) 50–62.

- [27] K.-C. Cheng, V. Acevedo-Bolton, R.-T. Jiang, N.E. Klepeis, W.R. Ott, O.B. Fringer, L.M. Hildemann, Modeling exposure close to air pollution sources in naturally ventilated residences: Association of turbulent diffusion coefficient with air change rate, Environ. Sci. Technol. 45 (9) (2011) 4016–4022.
- [28] T. Foat, J. Drodge, J. Nally, S. Parker, A relationship for the diffusion coefficient in eddy diffusion based indoor dispersion modelling, Build. Environ. 169 (2020) 106591.
- [29] J.S. Salinas, K. Krishnaprasad, N. Zgheib, S. Balachandar, Improved guidelines of indoor airborne transmission taking into account departure from the well-mixed assumption, Phys. Rev. Fluids 7 (6) (2022) 064309.
- [30] B. Chen, P. Jia, J. Han, Role of indoor aerosols for COVID-19 viral transmission: A review, Environ. Chem. Lett. 19 (2021) 1953–1970.
- [31] M.Z. Bazant, J.W. Bush, A guideline to limit indoor airborne transmission of COVID-19, Proc. Natl. Acad. Sci. 118 (17) (2021).
- [32] K. Choudhary, K. Krishnaprasad, S. Pandey, N. Zgheib, J. Salinas, M. Ha, S. Balachandar, Effectiveness of RANS in predicting indoor airborne viral transmission: A critical evaluation against LES, Comput. & Fluids (2023) 105845.
- [33] W. Wells, A. Contagion, A. Hygiene, An Ecological Study of Droplet Infections, Cambridge University Press, 1955.
- [34] L. Morawska, G. Johnson, Z. Ristovski, M. Hargreaves, K. Mengersen, S. Corbett, C.Y.H. Chao, Y. Li, D. Katoshevski, Size distribution and sites of origin of droplets expelled from the human respiratory tract during expiratory activities, J. Aerosol Sci. 40 (3) (2009) 256–269.
- [35] E. Riley, G. Murphy, R. Riley, Airborne spread of measles in a suburban elementary school, Am. J. Epidemiol. 107 (5) (1978) 421–432.
- [36] S.L. Miller, W.W. Nazaroff, J.L. Jimenez, A. Boerstra, G. Buonanno, S.J. Dancer, J. Kurnitski, L.C. Marr, L. Morawska, C. Noakes, Transmission of SARS-CoV-2 by inhalation of respiratory aerosol in the Skagit Valley Chorale superspreading event. Indoor Air 31 (2) (2021) 314–323.
- [37] L. Hamner, High SARS-CoV-2 attack rate following exposure at a choir practice— Skagit County, Washington, March 2020, MMWR Morb. Mortal. Wkly. Rep. 69 (2020)
- [38] K. Krishnaprasad, J. Salinas, N. Zgheib, S. Balachandar, Fluid mechanics of air recycling and filtration for indoor airborne transmission, Phys. Fluids 35 (1) (2023) 013344.
- [39] S.F. Arnold, Y. Shao, G. Ramachandran, Evaluating well-mixed room and near-field-far-field model performance under highly controlled conditions, J. Occup. Environ. Hygiene 14 (6) (2017) 427–437.
- [40] A. Vlachokostas, C.A. Burns, T.I. Salsbury, R.C. Daniel, D.P. James, J.E. Flaherty, N. Wang, R.M. Underhill, G. Kulkarni, L.F. Pease, Experimental evaluation of respiratory droplet spread to rooms connected by a central ventilation system, Indoor Air 32 (1) (2022) e12940.
- [41] J. Lee, S.-H. Park, G.-B. Sung, I.-H. An, K.-R. Lee, S.-P. Hong, S.-J. Yook, H.B. Koo, Effect of air cleaner on reducing concentration of indoor-generated viruses with or without natural ventilation, Aerosol Sci. Technol. 55 (11) (2021) 1288–1303.
- [42] R. He, W. Liu, J. Elson, R. Vogt, C. Maranville, J. Hong, Airborne transmission of COVID-19 and mitigation using box fan air cleaners in a poorly ventilated classroom, Phys. Fluids 33 (5) (2021).
- [43] A. Standard, Standard 55-1992, "Thermal Environmental Conditions for Human Occupancy". Atlanta: American Society of Heating, Refrigerating, and Air-Conditioning Engineers, Inc, 1992.